Caudal Intraparietal Sulcus and three-dimensional vision: a combined functional magnetic resonance imaging and single-cell study.

Amir-Mohammad Alizadeh[a], Ilse Van Dromme[a], Bram-Ernst Verhoef[b], Peter Janssen[a]

1. First name: Amir-Mohammad **Family name:** Alizadeh

a. Department of Neuroscience, Research Group Neurophysiology, O&N II Herestraat 49 - box 1021, 3000 Leuven, Belgium. Email: amir.m.alizade@gmail.com

2. First name: Ilse **Family name:** Van Dromme

a. Department of Neuroscience, Research Group Neurophysiology, O&N II Herestraat 49 - box 1021, 3000 Leuven, Belgium. Email: ilse.vandromme@icloud.com

3 First name: Bram-Ernst **Family name:** Verhoef

b. University of Chicago, Il, USA

verhoef@uchicago.edu

3. First name: Peter **Family name:** Janssen

a. Department of Neuroscience, Research Group Neurophysiology, O&N II Herestraat 49 - box 1021, 3000 Leuven, Belgium. Email: Peter.Janssen@kuleuven.be

Corresponding author: Dr. Peter Janssen, Department of Neuroscience, Research Group Neurophysiology, O&N II Herestraat 49 - box 1021, 3000 Leuven, Belgium

Tel/fax: +3216330669, Email: Peter.Janssen@kuleuven.be

- Authors declare no conflict of interests.

Abstract

The cortical network processing three-dimensional (3D) object structure defined by binocular disparity spans both the ventral and dorsal visual streams. However, very little is known about the neural representation of 3D structure at intermediate levels of the visual hierarchy. Here, we investigated the neural selectivity for 3D surfaces in the macaque Posterior Intraparietal area (PIP) in the medial bank of the caudal intraparietal sulcus (IPS). We first identified a region sensitive to depth-structure information in the medial bank of the caudal IPS using functional Magnetic Resonance Imaging (fMRI), and then recorded single-cell activity within this fMRI activation in the same animals. Most PIP neurons were selective for the 3D orientation of planar surfaces (first-order disparity) at very short latencies, whereas a very small fraction of PIP neurons were selective for curved surfaces (second-order disparity). A linear support vector machine classifier could reliably identify the direction of the disparity gradient in planar and curved surfaces based on the responses of a population of disparity-selective PIP neurons. These results provide the first detailed account of the neuronal properties in area PIP, which occupies an intermediate position in the hierarchy of visual areas involved in processing depth structure from disparity.

Keywords: Single unit recording, fMRI, binocular disparity, extrastriate cortex, macaque.

Acknowledgment: We thank Stijn Verstraeten, Christophe Ulens, Piet Kayenbergh, Gerrit Meulemans, Marc De Paep, Astrid Hermans, Sara De Pril and Inez Puttemans for technical and administrative assistance, and Steve Raiguel for comments on a previous version of this manuscript.We thank Mansoureh Fahimi, Elsie Premereur, Maria C Romero and Satwant Kumar for helpful discussions and assistance.

Funding: This work was supported by Fonds voor Wetenschappelijk Onderzoek Vlaanderen, Program Financing (PFV/10/008), IUAP VII/11 and Odysseus grant G.0007.12.

1. Introduction

The primate visual system needs to reconstruct the third dimension (depth) from a range of depth cues, among which binocular disparity – formed by positional differences between retinal images in the two eyes – is one of the strongest. The neural underpinnings of stereoscopic vision have been extensively studied in early visual cortex (Cumming and DeAngelis, 2001; Parker, 2007). A large number of studies have investigated the representation of 3D object structure defined by gradients of binocular disparity in the macaque inferotemporal (Janssen et al., 1999, 2000a, b; Yamane et al., 2008), posterior parietal (Srivastava et al., 2009; Theys et al., 2012b) and ventral premotor cortex (Theys et al., 2012a, 2013). In humans, a highly similar network has been described using fMRI (Ban and Welchman, 2015; Durand et al., 2009; Georgieva et al., 2008). More recently, considerable progress has been made in charting the anatomical connectivity of 3D-structure selective cortical regions in macaques (Premereur et al., 2015), in causally relating neural activity to perceptual performance in 3D structure categorization (Van Dromme et al., 2016; Verhoef et al., 2012), and even in clarifying the flow of visual information in this 3D-structure network (Janssen et al., 2017; Van Dromme et al., 2016). However, we know much less about the neural representation of 3D surfaces in intermediate areas of the dorsal and ventral visual stream (Orban, 2016). Detailed knowledge concerning neuronal properties in these mid-level areas may aid in understanding how these high-level representations are computed at the end-stages of the dorsal and ventral visual streams.

A previous monkey fMRI study (Durand et al., 2007) observed no significant 3D-structure related activations in the caudal Intraparietal Sulcus (IPS), although (Tsao et al., 2003) had reported strong disparity-evoked activations in this region evoked by near-far checkerboard stimuli. Recently however, another monkey fMRI study by Van Dromme et al., (2016) measured robust 3D-structure related activations in the caudal IPS in monkeys trained to discriminate 3D structure (concave vs convex). The activations related to 3D structure defined

by disparity were even more pronounced in the medial bank (area PIP) than in the lateral bank (area CIP). Moreover, the 3D-structure-selective patch in posterior AIP is effectively connected to both CIP and PIP (Premereur et al., 2015). Except for a few sporadic single-cell recordings (Sakata et al., 2005; Taira et al., 2000; Tsutsui et al., 2001), no study has investigated the properties of PIP neurons to date.

We combined fMRI-guided invasive electrophysiological recordings with advanced analytical methods to investigate the neural properties of the macaque area PIP in the medial bank of the caudal IPS. While a sizeable fraction of PIP neurons encoded the 3D orientation of planar surfaces (first-order disparities), only a very small proportion of PIP neurons exhibited selectivity for curved surfaces (i.e. second-order disparities). A linear support vector machine classifier could reliably decode the sign of curvature from a population of disparity-selective PIP neurons independent of position in depth, indicating that the population of PIP neurons contained significant information about 3D object structure. These results provide the first single-cell evidence regarding the role of area PIP in processing disparity gradients.

2. Materials and methods

2.1.Surgical procedures and animals

Three adult rhesus monkeys (two males and one female, ranging between 6.5-7.5 kg) served as experimental subjects for single-unit extracellular recordings. The monkeys were first implanted with an fMRI-compatible head post using dental acrylic and ceramic screws, under isoflurane anesthesia (Van Dromme et al., 2016). Monkeys were trained in a passive fixation task and a 3D-structure discrimination task previously described by (Verhoef et al., 2012). Two monkeys (R. and A.) were scanned during passive fixation of curved and flat surfaces, together with control stimuli for each condition (Van Dromme et al., 2016). We then implanted a

recording chamber vertically above the caudal part of the intraparietal sulcus, centered on the fMRI activation evoked by curved surfaces (contrast [*curved – control*] – [*flat – control*]) in monkeys R. and A., and at a similar anatomical position (Horsley-Clarke coordinates -10A and 8.5 L) in monkey B. Recordings were obtained from the left hemisphere of monkeys R and B and the right hemisphere of monkey A. Animal care and experimental procedures complied with the national and European guidelines (Directive 2010/63/EU) and were approved by the ethical committee of KU Leuven. Structural magnetic resonance imaging (MRI, 0.6 mm slice thickness), using glass capillaries filled with a 1% copper sulfate solution inserted into several grid positions, together with the pattern of grey to white matter transitions, confirmed that the recordings were made in the caudal part of the medial bank of the IPS, corresponding to area PIP. In addition, we obtained an anatomical MRI with the electrode in one of the recording positions for monkey A. (Figure 2A).

2.2.Stimuli

The animals were trained to maintain the gaze of both eyes inside an electronically defined 1° fixation window during the passive fixation task. Horizontal and vertical eye movements were recorded using an infrared camera system sampling at 500 Hz (EyeLink II; SR Research). After a 400 ms fixation period, the stimulus was presented for 600 ms at the fixation point (which remained visible), and if fixation had been maintained, a drop of juice was given as reward. During training and the single-cell recording experiments, stimuli were presented dichoptically using a double pair of ferroelectric liquid crystal shutters (optical rise/fall time about 35 µS, Displaytech) operating at a frequency of 60 Hz each and synchronized with the vertical retrace of the display monitor (20-in. P46 fast-decay phosphor; Vision Research Graphics), operating at a frequency of 120 Hz and at a viewing distance of 86 cm (Srivastava et al., 2009). Stimulus luminance measured behind the shutters (operating at 60 Hz) was 0.8 cd/m^2 with no measurable

cross talk between the images presented to the two eyes. All monkeys showed excellent stereopsis as demonstrated in an earlier 3D structure categorization test, in which concave and convex surfaces at different disparity coherences (ranging from 40 to 100% coherence) had to be discriminated by means of eye movements to the left or right (Verhoef et al., 2012).

We used a basic stimulus set consisting of 32 pairs of disparity-defined curved surfaces, which was identical to that used by (Srivastava et al., 2009), together with eight planar surfaces (first-order stimuli). The first-order stimuli (Figure 1A) were presented in two different sizes (8.3° and 18.7°, except for monkey B where we used only the 8.3° planar stimuli), and consisted of squares with linear disparity gradients either along the vertical or horizontal axis of the stimulus (50% dot density). The surfaces in which disparity varied along the vertical axis (30° rotation along the horizontal axis) could have the top tilted either towards (profile A) or away from the observer (profile B). Similarly, the surfaces in which disparity varied along the horizontal axis could have the right side towards (profile A) or away from the observer (profile B). The two profiles were derived from the same monocular images by simply interchanging the images presented to each eye. To avoid texture-density cues in surfaces with disparity variations along the horizontal axis, we randomly removed dots with each change in disparity, as in previous studies (Janssen et al., 2001). The curved (second-order) surfaces (Figure 1B) were constructed by combining four pairs of depth profiles (half-sine, inclined, Gaussian, S-shape) with eight two-dimensional (2D) shapes, filled with a 50% density random-dot pattern. The combination of a 2D contour and a depth profile generates a 3D stimulus. The two members of each 3D surface pair used the same two monocular images, since interchanging the monocular images between eyes yielded two 3D surfaces that differed only in the signs of their disparity gradients (convex surfaces become concave and vice versa). The curved surfaces measured 6.6° vertically, dot size was 2 arcmin, and stimulus contrast was 4.6 ($\Delta I/I$). In the case of the curved stimuli, disparity varied only along the vertical axis of the stimulus.

2.3.fMRI experiment: scanning procedures and stimuli

All scanning procedures have been described in Van Dromme et al. (2016). We trained monkeys A. and R. to sit in a sphinx position inside an MRI-compatible plastic chair, which was placed inside the horizontal bore of the magnet. Stimuli were projected using a digital projector (Barco 6300 LCD) onto a translucent screen positioned 57 cm in front of the monkey. A pair of red/green stereo-glasses were placed in front of the monkey's eyes to provide dichoptic presentations of the stimuli. We used a 3.0 Tesla full body scanner (Trio, Siemens), and a radial transmit-only surface coil and custom-built eight-channel phased-array receive coil were positioned closely around the monkeys' head. A contrast agent (monocrystalline iron oxide nanoparticle or MION; Feraheme, AMAG pharmaceuticals) was injected to enhance the signal-to-noise ratio and spatial selectivity of the MR signal (Zhao et al., 2006). We used a gradient-echo single-shot T2 – weighted echo-planar imaging sequence (40 horizontal slices, TR=2 s, TE =17 m, 1.25 mm isotropic). A pupil/corneal reflection tracking system (Iscan, operating at 120 Hz) was used to monitor the position of one eye. Monkeys were required to maintain fixation on a dot on the center of screen within a 1.5° electronically-defined window.

We used a 2 by 2 block design with factors *curvature* (curved versus flat) and *disparity* (stereo versus control). In the curved stereo condition, we presented a subset of the curved surfaces (four 2D shapes and three pairs of depth profiles, Van Dromme et al., 2016) at two positions in depth. In the flat stereo condition, we presented flat surfaces (with the same 2D contours) at 12 positions in depth such that the disparity content (i.e. the sum of all disparities) was identical to the one in the stereo curved condition. The curved-control and flat-control conditions consisted of the presentation of one of the monocular images of the corresponding stereo conditions to both eyes simultaneously.

2.4.Single-cell experiment

During all single-unit recording sessions, eye position signals from both eyes, neural activity, and photocell pulses were digitized and processed at 20 kHz on a digital signal processor (DSP) (C6000 series; Texas Instruments). Extracellular neural activity was recorded by means of tungsten microelectrodes (1MΩ, FHC , USA). After amplification (1000 times), the signal was passed through an analogue band-pass filter (500-5000 Hz), and then sent to the digital signal processor. Single-unit activity (spikes) was discriminated on-line on the DSP using a dual-time window discriminator and displayed using LabView and custom-made software.

The search test consisted of 32 curved stimuli (8 different shape contours combined with 4 different 3D profiles) in addition to 8 planar surfaces (linear disparities in two sizes as described above). We collected at least 6 correct trials per condition (median = 8) during the search test. If a unit was well-isolated and responsive to at least one of the stimuli in the search test, we presented two pairs of planar stimuli as well as two pairs of curved surfaces with identical 2D contours, selected on the basis of the responses observed in the search test (one stimulus to which the neuron fired strongly and one less-effective stimulus). In addition, we showed the monocular images of the same stimuli to the left and the right eye separately (disparity test). The most effective stimulus was labelled the preferred 3D surface; the other member of that pair (with identical 2D contour but opposite depth profile) was termed the nonpreferred 3D surface. Stimuli were presented at the center of the display (at the fixation point) and at the middle position- in-depth (mean disparity 0).

If a neuron showed significant response differences between the members of a pair of 3D surfaces that could not be accounted for by the sum of the monocular responses, the pair of

3D surfaces evoking the strongest selectivity was studied further in the position-in depth test (PID test). In this test, the preferred and the nonpreferred stimuli were displayed at five positions in depth at the fixation point. The average disparity varied from -0.5° (near) to +0.5° (far), which was a wider range than the disparity amplitude in the stimulus (0.65°). Because the disparity in the stimulus varied between -0.83° and -0.18° for the extreme near position in depth, and between +0.18º and +0.83° for the extreme far position in depth, the stimulus consisted entirely of either near or far disparities at the extreme positions in depth. For the position-in-depth test, it was critical to measure changes in vergence angle after stimulus onset, since vergence eye movements tracking the stimulus in depth could potentially reduce the variation in the mean disparity of the test. Therefore, we measured the positions of both eyes in this test. At the beginning of every recording session, we calibrated the eye position signal by presenting the fixation point (without the stimulus) at two positions on the horizontal meridian 4° from the center of the display.

To assess the neural selectivity for stimulus size, we presented the preferred and nonpreferred stimuli at 8 different sizes (Size Test): 4.1°, 6.25°, 8.3°, 10.4°, 12.5°, 14.6°, 16.6° and 18.75°. All stimuli in the size test were presented foveally at the fixation plane and all stimulus parameters (except size) were identical to those in previous tests.

To assess the receptive fields of the neurons, we presented the preferred stimulus with a size of 3.7° at 35 positions on the screen (on a 7 by 5 grid), spaced 3.83° apart on the horizontal axis and 4.26° on the vertical axis, covering an area of 17° by 23° around the fixation point (Receptive field test). Each stimulus was presented for 400 ms during passive fixation.

2.5.Data analyses

The analysis of the fMRI data has been described in Van Dromme et al. (2016). Briefly, depth-structure sensitivity was defined as a significant interaction ($p < 0.05$ family-wise error rate corrected, FWE for multiple comparisons on the entire brain) between the factors *curvature* (curved or flat) and *disparity* (stereo or control) in the block design. Both monkeys showed a significant fMRI activation related to depth-structure sensitivity in the medial bank of the caudal IPS, corresponding to area PIP, which was then used to guide the implantation of the recording chamber.

Data analysis was performed using MATLAB 2015b (Mathworks). We calculated net neural responses by subtracting the mean activity in the 300 ms immediately preceding stimulus onset from the mean activity between 40 and 540 ms after stimulus onset. In the search test, we performed a t-test (at $p = 0.05$ corrected for 40 conditions) on the neuron's response to each condition to determine the responsiveness of the neuron.

In the disparity test, a two-sample t-test was applied to the responses elicited by the two members of each pair of 3D stimuli to assess disparity selectivity. To verify that the observed selectivity did not reflect selectivity for the monocular images, we calculated a stereo difference index (SDI) (Srivastava et al., 2009) : $SDI = \frac{D\ stereo - D\ Mono}{D\ stereo + D\ Mono}$ in which D_{stereo} represents the response difference between preferred and nonpreferred 3D surface in the stereo condition, and D_{mono} represents the difference in the sum of the monocular responses . If the SDI was greater than 0.5, the stereo selectivity was considered to arise from binocular rather than monocular mechanisms (Srivastava et al., 2009). To quantify the degree of stereo selectivity, we calculated a stereo selectivity index (SSI) on the responses to the 3D surface pair yielding the highest selectivity as follows: $SSI = \frac{R_B - R_W}{R_B}$, in which R_B is the response to the best 3D surface and R_W is response to the worst 3D surface. Population response latencies were calculated by identifying the first of three 10 ms time bins in which the population response to the preferred

3D surface was significantly higher than in the preceding time bin (t-test, $p \leq 0.05$). The population latency of the neural selectivity was likewise computed as the first of three 10 ms time bins in which the population response to the preferred 3D surface significantly exceeded the response to the nonpreferred 3D surface (t-test, $p \leq 0.05$). In addition, we computed the response latency for each individual neuron using the Poisson cumulative distribution (Janssen et al., 2008).

In a manner similar to previous studies (Janssen et al., 2000a; Srivastava et al., 2009; Theys et al., 2012b), we assessed whether the neural selectivity observed in the disparity test reflected selectivity for gradients of disparity (rather than for zero-order disparity) by presenting the preferred and nonpreferred surface at 5 positions in depth. As a criterion we required that the response to the nonpreferred 3D surface should never significantly exceed any of the responses to the preferred 3D surface in the position-in-depth test. To characterize every neuron tested, we compared the neural selectivity at the middle position ($\mathrm{SSIm} = \frac{Pref-Null}{Pref}$, in which 'Pref' and 'Null' are the responses to the preferred and nonpreferred conditions at the fixation plane), to the neural selectivity at the worst position ($\mathrm{SSI_w}$, i.e., the minimum response to the preferred stimulus minus the maximum response for the nonpreferred stimulus divided by the response to the preferred stimulus at the middle position, (Janssen et al., 2000a)).

We constructed receptive field (RF) maps using cubic two-dimensional interpolation of the net responses measured in the RF test. We subtracted the standard deviation (SD) from the maximum response of the neuron and plotted the contour corresponding to the maximum response – 1 SD on the RF maps. To verify the consistency of the receptive field maps, we divided the trials into even and odd trials and calculated the correlation coefficient between the two sets of trials.

In order to assess which 3D information can be reliably extracted from neuronal activity in area PIP, we used a linear support vector machine (SVM, the neural decoding toolbox ver. 1.0.4, http://www.readout.info/). Meyers et al., (2008) have described details of this toolbox and the classification analysis procedures. We used the position-in-depth test data of 40 disparity-selective neurons tested with vertical linear disparity gradients and 40 cells tested with curved stimuli (25 neurons included in this analysis were tested with both curved and planar stimuli). We only considered vertical linear disparity gradients because the labels of the stimuli should be unambiguous for the SVM analysis, and because most neurons in PIP were selective for planar surfaces with vertical gradients. We selected cells with at least 20 trials per condition and if a condition had more than 20 trials, we randomly selected 20 trials. For each neuron, data from 10 trials from each of the ten conditions (PID test, consisting of either a pair of concave/convex or A/B profiles at 5 positions in depth, so 2×5 = 10 conditions) were randomly selected. For each of these trials, 500 ms of neural activity after stimulus onset from all neurons was combined to create a psuedopopulation response vector for PID tests with curved stimuli and planar stimuli independently. This procedure resulted in 10×10 data points in a 40-dimensional space. These pseudopopulation vectors were grouped into 10 splits of data with each split containing one pseudopopulation response vector for each of the 10 stimuli. Nine of these splits were used to train the pattern classifier (linear SVM) whereas the remaining one was used to test the performance of the classifier (10-fold cross-validation). A z-score normalization was applied in a trial-by-trial approach before sending data to the classifier. Classification was performed for the sign of the disparity gradient and the position-in-depth of the stimuli separately. Chance level was estimated by averaging the results of running the classifier 1000 times with the labels randomly shuffled, with permutation of the order of neurons and the selection of trials for training and testing. All classification accuracy values presented in this paper are the zero-one loss function results (proportion of correct predictions),

and the standard error (SE) is expressed as the standard deviation across *n* number of resample runs. In order to assess how well the 3D structure information (sign of the disparity gradient) at a given mean disparity value generalized across position in depth, we trained the classifier with a concave/convex pair (or profile A or B for planar stimuli) at one position in depth, and tested on each of the other positions in depth independently.

3. Results

3.1. fMRI activations related to 3D structure sensitivity in the caudal IPS

We scanned two monkeys (R. and A.) during presentation of curved and flat surfaces at the fixation point (127 and 125 runs for R. and A., respectively). The contrast [(curved stereo – curved control) – (flat stereo – flat control)] yielded robust ($p < 0.05$ corrected) and bilateral activations in the caudal IPS of both animals (Figure 2). In monkey A., these 3D-structure related activations were located mainly in the medial bank of the caudal IPS (Figure 2A), close to the fundus of the IPS, and largely corresponding to area PIP (Lewis and Van Essen, 2000; Rosenberg et al., 2013; Van Dromme et al., 2016). Monkey R. showed stronger activations in the caudal IPS that included both the medial (area PIP) and the lateral bank (area CIP) of the caudal IPS (Figure 2D). Thus, the medial bank of the caudal IPS (area PIP) showed strong sensitivity for depth structure in fMRI in both monkeys, consistent with Van Dromme et al. (2016). Note, however, that our curved surfaces contained both first-order (linear) disparity gradients (e.g. the top part of a convex surface) and second-order (curved) disparity gradients. Therefore, the fMRI results do not allow us to draw conclusions about first- or second-order disparity selectivity at the single-neuron level in area PIP.

The top panels in Figure 2B and D illustrate the recording positions mapped onto the fMRI activations on horizontal sections through the caudal IPS. Because of the complex folding of the caudal IPS, some recording positions may appear to have been targeting the lateral bank of the IPS, but extrapolation of the recording tracks verified that we did reach the medial bank of the caudal IPS as the electrode was

lowered (see electrode in one recording position in Figure 2A). The same complex folding of the caudal IPS prevented us from precisely mapping the properties of individual neurons onto the fMRI activations. Therefore, the top right panels in Figure 2B and D merely illustrate that our recording positions were located within the fMRI activations. In the anterior IPS, which is anatomically much less complicated compared to the caudal IPS, it is possible to identify the neuronal selectivity per recording position across a large region of cortex (Van Dromme et al., 2015).

3.2. Disparity selectivity of single neurons in functional- defined area PIP

In total, we recorded activity in 101 responsive PIP neurons in three monkeys (B., A. and R., the latter animal was previously used in (Van Dromme et al., 2016)), in the fMRI activations elicited by curved surfaces (in monkey A. and R.) and in an anatomically corresponding region in monkey B. The example neuron in Figure 3A fired strongly (50 spikes/sec on average) to one of the planar surfaces (tilted top part towards the observer, 30°), and showed an inhibitory response to its counterpart composed of the same two monocular images (tilted top part away from the observer, SSI = 1.4). The monocular responses could not account for this selectivity (SDI = 1.3), and two other planar surfaces (with zero tilt and slant = -30 and +30°) did not evoke any response. When tested with curved surfaces (Figure 3B), this example neuron also showed significant – albeit weaker – selectivity (SSI = 0. 63) for both pairs of curved stimuli, which could not be accounted for by the monocular responses. Thus, this example PIP neuron exhibited disparity selectivity both for planar surfaces and for curved surfaces.

The substantial majority of PIP neurons tested with planar surfaces (74/101, 73%) showed significant response differences that could not be explained by the monocular responses. The average population response of those 74 neurons is illustrated in Figure 3C. Planar surfaces elicited very robust and selective responses (population SSI = 0.96), whereas the monocular presentations were much less effective. Remarkably, our population of selective PIP neurons began signaling differences in 3D orientation between planar surfaces as early as 45 ms after stimulus onset (first of three consecutive 10 ms bins with significant response differences between preferred and nonpreferred surface). The median

response latency, as calculated for every individual neuron, averaged 55 ms across the population (Poisson statistic). In addition, a smaller but sizeable proportion of the neurons (54/94, 57%) showed selectivity for curved surfaces, as illustrated in Figure 3D. Compared to planar surfaces, the degree of selectivity (SSI = 0.81) was lower and the response latency longer (60 ms) for curved surfaces. The latency of selectivity onset for the population of disparity-selective cells was 55 ms (first of three significant bins, t-test, n=74) for planar surfaces and 65 ms for curved stimuli (n=54). The distribution of the SSI for planar and for curved surfaces is illustrated in Figure 3E. The neuronal selectivity for planar surfaces was not significantly correlated with that for curved surfaces ($r = 0.1$, $p = 0.65$).

Response variations for different 3D surfaces do not necessarily imply selectivity for gradients of disparity (Janssen et al., 2000b). To evaluate this higher-order disparity selectivity, we tested PIP neurons with 3D surfaces presented at 5 different positions in depth. The example neuron in Figure 4A (the same neuron as in Figure 3) preserved its selectivity for tilted planar surfaces at every position in depth ($p < 0.01$ for the difference between preferred and nonpreferred surfaces at every position), although the mean disparity of the stimulus did affect the absolute response level of the neuron (ANOVA on the responses to the preferred surface, $p < 0.001$). Since the response to the nonpreferred planar surface never significantly exceeded the response to the preferred planar surface, this neuron was deemed higher-order disparity selective. As in previous studies (Srivastava et al., 2009), vergence eye movements could not account for the neural responses, since the eyes remained stable throughout the first 200 ms after stimulus onset (Figure 4C) though neural selectivity was clearly present. Moreover, the average deviation of the eyes (0.15°) was much smaller than the range of disparities in the test. When tested with curved surfaces (Figure 4B), this neuron preserved its selectivity in 4 out of 5 positions-in-depth tested, and its selectivity did not invert for any of the positions tested, indicating a higher-order disparity selectivity. However, because planar (first-order) stimuli were sufficient to elicit selective responses, we considered this example neuron to be first-order disparity selective, in agreement with previous studies (Janssen et al., 2000b; Theys et al., 2013).

The response pattern of the example neuron was highly representative of the population of disparity-selective PIP neurons. In total, we ran a PID test in 91 disparity-selective neurons, 30 of which

were tested with both planar and curved surfaces. Sixty-nine were tested with planar surfaces, 52 with curved surfaces. Out of the 69 disparity-selective PIP neurons tested with planar (first-order) surfaces, 26 (42% in total; 53%, 46% and 29% in monkeys B., R. and A, respectively) were higher-order disparity selective. However, only 11 neurons (out of 52 neurons tested, 21%) were higher-order disparity selective for curved stimuli, and 5 of those neurons were also higher-order when tested with planar stimuli (and therefore deemed to be first-order). Thus, only a very small minority of PIP neurons (6/52 or 12%) were higher-order disparity selective for curved surfaces but not for first-order surfaces. In contrast, 5/10 neurons tested preserved their selectivities across position in depth for planar surfaces but not for curved surfaces. The remaining 59 neurons (out of 91 neurons tested, 65%) were zero-order cells (Table 1). Figure 5A and B illustrates the average responses of all higher-order PIP neurons to planar and curved stimuli, respectively. At the population level, the response differences between preferred and nonpreferred planar and curved surfaces were significant at every position in depth ($p < 0.01$). Note that the average selectivity for planar surfaces was stronger at far disparities, whereas the average selectivity for curved surfaces was stronger at near disparities (Figure 5A and B). We can only speculate that this difference could be related to the processing of (large) planar surfaces (e.g. a tabletop), in which far disparities are important, as opposed to the processing of curved surfaces (as in graspable 3D objects), for which near disparities may be more relevant.

The majority of the first-order neurons (18/26) were selective for the vertical disparity gradients. Moreover, 40% of all disparity-selective PIP neurons (30/74) discriminated reliably between vertical and horizontal disparity gradients at the fixation plane (t-test between the highest response to a vertical disparity gradient and the highest response to a horizontal disparity gradient, $p< 0.05$).

To characterize the response behavior of every neuron tested with 3D stimuli at different positions in depth, we calculated two selectivity indices (SIs): the SI_{middle}, which quantifies the selectivity at the fixation plane (which was also used in the preceding tests,), and the SI_{worst}, which compares the lowest response to the preferred surface (at any of the positions tested) to the highest response to the nonpreferred surface in the test (see methods). Figure 5C shows a scatter plot of these two indices for all neurons tested (N = 75). The subpopulation of zero-order neurons (red symbols) exhibits negative

SI_{worst} values, whereas first-order neurons (blue symbols) have SI_{worst} values near or above zero. The average vergence eye movements were small (0.2° divergence at the far positions) and occurred relatively late (approximately 200 ms after stimulus onset) in the trial (data not shown).

In order to relate our single-cell data to the fMRI activations, we compared the average responses to planar and curved surfaces at the three middle positions in depth (the same range as used in Van Dromme et al., 2016) to the responses to flat surfaces at the same positions in depth for all disparity-selective PIP neurons tested with planar, curved and flat surfaces (N = 56, Figure 5D). The mean response to curved and planar stimuli across the three positions in depth was significantly higher than that to flat stimuli (t-test, $p < 0.01$), and there was no significant difference between the average responses to planar and curved stimuli. With the caveat that we did not search for responsive neurons using flat stimuli (which may have introduced a bias in the selection of neurons), the population of PIP neurons that we tested may have contributed to the stronger fMRI activation for curved surfaces than for flat surfaces at different positions in depth.

3.3. Selectivity for stimulus size and receptive fields of PIP neurons

The planar surfaces in our study were relatively small (8.3° diameter), but previous studies in neighboring area CIP have used very large planar surfaces (e.g. 53° in (Rosenberg et al., 2013)). Therefore, we also wanted to investigate to what extent PIP neurons preserve their selectivities across size variations for planar stimuli presented at the fixation point. The example neuron in Figure 6A was highly selective across a 4.5-fold size range (from 4.1° to 18.75° diameter, t-test on the difference in response to preferred and nonpreferred surfaces for all except 4.1° and 6.2°, $p < 0.02$). However, stimulus size significantly affected the neuronal response (ANOVA, main effect of size $p = 0.004$) and showed some interaction with the neuronal selectivity (ANOVA, interaction between 3D profile and size $p = 0.06$). We examined the effect of stimulus size on the 3D preferences of 40 disparity-selective (based on the disparity test) PIP neurons. Almost all neurons (36/40, 90 %) showed some degree of size invariance for 3D preference, i.e. were selective for more than one stimulus size (average number of

sizes with selectivity = 4). Figure 6B illustrates the average responses to preferred and nonpreferred planar surfaces across eight different sizes. Overall, larger sizes evoked stronger responses in PIP (specifically the 16.6° and the 18.7° stimuli), but the neuronal response to the preferred profile was always significantly greater than the response to the nonpreferred profile, even for the smallest size. Thus, PIP neurons do not require large 3D surfaces to exhibit selectivity.

Because most PIP neurons responded to the smallest size tested (4.1°), we mapped the receptive fields of 40 PIP (zero- and first-order) neurons with the preferred stimulus (diameter 3.7°, to avoid overlap between neighboring positions) at 35 positions in the central visual field (covering a 17° × 23° area around the fixation point) and at the fixation plane (center position in depth). The example neuron in Figure 7A responded weakly at the fixation point (6.5 spikes/sec), but fired much more strongly to stimulus presentations in the lower visual field (82 spikes/sec), yielding an RF with a single local maximum. In contrast, the neuron in Figure 7B responded maximally near the fixation point in the contralateral hemifield, but also showed a second maximum in the ipsilateral hemifield (i.e. a multifocal RF). The neuron in Figure 7C is another example of a multifocal RF, with two maxima in both the ipsi- and contralateral hemifields separated by an area with strong inhibitory responses (notice the scale bar in Figure 7C). The average RF in our population of PIP neurons was bilateral and measured 236 degrees^2 (Figure 7D). Most PIP neurons tested (35/40, 87.5 %) showed more than one local maximum in the RF, and most (31/40) also showed significant ipsilateral responses. Only 2 neurons (5%) responded maximally at the fixation point, with nearly equal proportions showing a maximum in the contralateral (18/40) or ipsilateral (17/40) hemifield. The remainder of the neurons (8/40) responded maximally at the vertical meridian outside the fovea, as with the example neuron in Figure 7A.

A smaller fraction of the neurons (N=15) were also tested with the preferred surface at three positions in depth. To quantify the consistency of the RF profile across position in depth, we calculated the 2D correlation coefficients between the three positions in depth tested (near – center, center – far). Because this population of PIP neurons contained many zero-order neurons (N=11), which did not preserve their selectivity across position in depth, the 2D correlations were relatively modest (near-center: median r = 0.35, far-center median r = 0.49).

The combined results of the size test and the RF test clearly illustrate how stimulus size and position interact. The stronger responses to larger stimulus sizes (presented at the fovea) in the size test could at least partially be explained by the observation that the RFs of most PIP neurons have parafoveal centers. Moreover, the RF test also demonstrates that PIP neurons do not require large surfaces, since we measured very strong responses (average maximum response in the RF test = 30 spikes/sec) even with stimuli measuring merely 3.7°.

3.4. Decoding of 3D structure and position in depth

To determine whether a population of 40 disparity-selective PIP neurons tested with planar stimuli (vertical disparity gradients only) and 40 cells tested with curved stimuli (both populations included zero- and higher order neurons) contains reliable information regarding first and second-order disparities (convex – concave, or profile A and B) across positions-in-depth, we used a linear SVM classifier (see Methods). We classified both the sign of the disparity gradient (profile A vs B, or concave vs convex) and the position in depth of the stimulus based on the neuronal responses of these neurons. For determining the sign of the disparity gradient, we randomly selected trials from all five different positions in depth and used concave/convex as labels for tests with curved stimuli, and profile A/B as labels for test with planar stimuli. For planar stimuli, classification accuracy was close to perfect (0.99 ± 0.06 over cross-validations over resample runs). Interestingly, despite a very small number of second-order neurons in our sample, the classification performance was very similar for curved surfaces (0.99 ± 0.05) (Figure 8A). For comparison, we ran the classifier on the same population of PIP neurons to decode position in depth (near, fixation plane, and far). Although classification accuracy was slightly lower for planar stimuli (0.85±0.19) and for curved stimuli (0.85±0.19), the classifier still performed significantly above chance level for decoding position in depth for both types of stimuli (Figure 8B). Thus, at the population level, PIP contains information about first-order and second-order disparities across positions-in-depth and about position-in-depth. To determine how well 3D structure information extracted at any given position in depth might generalize to other positions in depth, we trained the

classifier with the concave-convex pair (or A-B pair in case of planar stimuli) at each position in depth (separately) and tested the classifier at all other positions. Results of the classification on the responses to the planar stimuli (Figure 8C) indicate that information about the sign of the disparity gradient reliably generalizes across all positions in depth ($p < 0.05$ for all combinations of positions in depth, figure 8C). For curved surfaces, the performance of the classifier was quite similar except for the extreme positions in depth. Notably, the 3D structure information extracted from the extreme far position (+0.5) generalized only to its neighboring position in depth (+0.25) but could not be used to detect the sign of curvature at any other position in depth (Figure 8D). As a control, we repeated the SVM analyses using a Gaussian kernel. The classification performance for the sign of the disparity gradient and position in depth improved slightly (2-3% improvement). However, the generalization performance for the planar stimuli was much weaker compared to the linear classifier (Supplementary Figure 1) whereas the generalization for curved surfaces remained largely unchanged. Thus, a linear classifier provided optimal classification of the stimuli based on the PIP responses. Given the range of mean disparities in the fMRI studies (-0.5° to +0.5°), we observed reliable decoding of higher-order disparity information, at the population level, across a similar range in area PIP.

To verify that the SVM classifier did not rely exclusively on the contribution of a small number of highly selective neurons, we repeated the SVM analysis after exclusion of the 25% most selective neurons in our sample (N=30 instead of 40). The performance of the SVM classifier was still well above chance level (0.84 and 0.83 correct for the sign of the disparity gradient and 0.66 and 0.56 correct for position in depth for planar and curved stimuli, respectively), indicating that the SVM result did not depend on the presence of a small number of selective neurons (Supplementary Figure 2).

To investigate which neurons were most informative for the classifier, we calculated the correlation between the weights assigned to each neuron multiplied by the average neuronal response and the disparity selectivity of the neuron (the SSI at the middle position in the PID test), and between the weights × neuronal response and the number of positions in depth at which the neuron was selective (a measure of higher-order disparity selectivity). All correlations were low to moderate: for disparity selectivity $r = 0.05$ ($p = 0.74$) for planar stimuli and $r = -0.32$ ($p = 0.04$) for curved stimuli, for numbers

of positions in depth: r = 0.35 (p = 0.03) for planar stimuli and r = -0.09 (p = 0.57) for curved stimuli. However, the interpretation of the weight vectors may be difficult (see Haufe et al., 2014).

4. Discussion

The current study is the first single-cell investigation of the properties of neurons in area PIP, in a region that had been more strongly activated by curved surfaces than by flat surfaces in an fMRI experiment. With the exception of a very small number of second-order neurons, PIP neurons were either zero-order (coding merely position in depth) or first-order (coding the tilt and slant of planar surfaces) disparity-selective. The centers of the receptive fields in PIP were mostly located parafoveally in the contralateral hemifield, often with a second focus in the ipsilateral hemifield. The results clearly distinguish PIP from other extrastriate areas that are sensitive to the disparity-defined depth structures of objects.

Our findings are also relevant with respect to the organization of the intraparietal sulcus areas in humans. The putative human homolog of area CIP in the monkey has been designated VIPS, IPS0 (Konen et al., 2013) or the V7/V7A cluster (Orban, 2016). Recently, Orban (2016) suggested that the caudal IPS might contain two areas, VIPS (which may correspond to CIP in the monkey) and POIPS (located more medially). Here, we provide the first single-cell evidence for neuronal disparity selectivity in area PIP, in the medial bank of the caudal IPS neighboring area CIP (Tsutsui et al., 2002). Thus, in both monkeys and humans, the caudal IPS may harbor two areas sensitive to disparity gradients (Shikata et al., 2008).

fMRI provides an indirect measure of neuronal activity (Logothetis et al., 2001), but is invaluable for constructing a map of activity across the entire macaque brain so that single-cell recording experiments can be precisely targeted to regions of interest (Popivanov et al., 2012; Theys et al., 2012b; Tsao et al., 2003; Van Dromme et al., 2015). Our fMRI experiment contrasted the activations elicited by curved disparity-defined surfaces (curved stereo condition) with the activations elicited by flat surfaces at different disparities (flat stereo

condition), after subtracting the activations evoked by the respective monocular images. Since the disparities were exactly matched between the curved stereo condition and the flat stereo condition, any differences in fMRI activations must have resulted from a sensitivity to gradients of disparity. A previous study (Van Dromme et al., 2016) using the same stimuli observed an extensive network of cortical regions sensitive to disparity gradients, comprising several patches in posterior (PIT) and anterior IT (AIT), as well as in PIP, CIP and AIP in the intraparietal sulcus, and F5a in ventral premotor cortex. Single-cell experiments confirmed the presence of first- and second-order neurons in AIT, AIP and F5a (Janssen et al., 2000a; Srivastava et al., 2009; Theys et al., 2012a; Van Dromme et al., 2016). The current study is the first to demonstrate higher-order disparity selectivity in a mid-stage, fMRI-defined node of the 3D shape network located between early visual areas, which mainly encode absolute disparity (Cumming and DeAngelis, 2001) and relative disparity (Thomas et al., 2002), and the higher-tier areas AIT, AIP and F5a. However, curved surfaces also contain components of first-order disparity gradients (e.g. the top and bottom parts of a convex surface). Hence, the fMRI activation evoked by curved surfaces may have been induced by the underlying first-order selectivity in PIP. Although we did observe some neuronal selectivity for curved surfaces in PIP, we consider it unlikely that the strong fMRI activations arose from a very small number of second-order neurons in PIP. Furthermore, on average, at least the PIP neurons that we recorded responded more strongly to curved surfaces than to flat surfaces (Figure 5D), which may also have contributed to the fMRI activation. Obviously, the fMRI block design we used in previous studies cannot furnish the same detailed assessments of neuronal selectivity we can achieve with single-cell recordings.

The decoding analysis showed very good classification performance for the 3D orientation of planar surfaces, and, despite a very small number of second-order neurons, for the sign of the disparity variation (convex or concave) in curved surfaces. Thus, at the

population level PIP contains reliable information regarding the 3D structure of curved surfaces. Similarly, we observed very good classification performance for position in depth (near, fixation plane, far) for both curved and planar stimuli, which was not surprising given the fact that a large proportion of our PIP population were zero-order, and almost all PIP neurons were significantly affected by position in depth. The generalization analysis performed with the classifier trained at one position in depth and tested at all other positions confirmed that at the population level, PIP is position-invariant for the 3D orientation of planar surfaces and for the 3D structure of curved surfaces.

PIP contains a largely implicit representation of second-order disparity, as opposed to the explicit (position-invariant) representations of second-order disparity in individual neurons in areas AIT (Janssen et al., 2000b), AIP (Srivastava et al., 2009) and F5a (Theys et al., 2012a). It is possible that this implicit representation was detected in the fMRI contrast we used (curved surfaces at different disparities minus their control stimuli compared to flat surfaces at different disparities minus their control stimuli, (Van Dromme et al., 2015)). A similar phenomenon may exist at the level of area V4, which is strongly activated by curved surfaces (Van Dromme et al., 2016) although previous monkey single-cell studies have indicated that V4 neurons do not preserve their selectivity across position in depth (Hegde and Van Essen, 2005). Similarly, human fMRI data suggest that area V3A in humans contains a representation of surface slant that is to some degree tolerant to changes in position (Ban and Welchman, 2015), whereas monkey single-cell data (Anzai et al., 2011) suggest a mere coding of absolute disparity in area V3A. However, the inter-species comparison in the latter studies warrants caution in light of apparent discrepancies between fMRI and single-cell data mentioned previously. Future studies in monkeys combining fMRI and single-cell recordings should clarify whether the fMRI signal is effectively more sensitive to implicit representations of stimulus features.

The robust neuronal selectivity for tilted and slanted planar surfaces and the weak selectivity for curved surfaces in PIP suggest that the properties of PIP neurons are similar to those in neighboring area CIP (Katsuyama et al., 2010; Rosenberg and Angelaki, 2014a, b; Rosenberg et al., 2013; Tsutsui et al., 2001; Tsutsui et al., 2002), with which PIP is strongly interconnected (Van Dromme et al., 2016). However, we could also identify a number of intriguing differences between these two caudal IPS areas. Both CIP and PIP are strongly connected to other parietal areas belonging to the dorso-dorsal (V6, V6A) and the ventro-dorsal (LIP) pathway, but only the 3D-shape sensitive region in PIP is connected to V3 and V3A (Van Dromme et al., 2016). Moreover, the response latencies of PIP neurons are relatively short (50 ms on average) and PIP RFs tend to be moderate in size (240 deg^2), whereas in area CIP, response latencies are longer (60-70 ms) and RFs tend to be larger (Rosenberg, personal communication). Finally, PIP neurons are frequently zero-order disparity selective, whereas CIP neurons are rarely zero-order disparity selective (Rosenberg, personal communication). Overall, this pattern of results seems to suggest that area PIP occupies a position in the hierarchy of visual areas that is earlier than that of area CIP. Given that earlier visual areas V3 and V3A predominantly encode absolute disparity and not relative disparity, area PIP may be the first cortical area that hosts neurons selective for gradients of binocular disparity (Orban, 2011). An alternative view is that PIP and CIP are both mid-level visual areas important for the computation of disparity gradients, and that PIP predominantly feeds into the dorso-medial pathway for reaching (Bosco et al., 2010; Hadjidimitrakis et al., 2012) whereas CIP feeds into the dorso-lateral pathway for grasping (Murata et al., 2000; Nakamura et al., 2001). In this interpretation, the weak selectivity for curved surfaces in PIP is not surprising, since curvedness is an object property that can determine the preshaping of the hand during grasping but is not essential for reaching. The higher proportion of zero- and first-order neurons, on the other hand, may be useful for planning reaching movements in depth (Hadjidimitrakis et al., 2014). It is

also noteworthy that the receptive fields of PIP neurons rarely included the fovea, but were frequently bilateral and symmetrical around the fovea. In contrast, RFs in AIP are mostly centered on the fovea (Romero and Janssen, 2016). Since recent studies have revealed that grasping signals are also present in the dorso-medial pathway (Fattori et al., 2010) and reaching signals can be measured in the dorso-lateral pathway (AIP, Lehmann and Scherberger, (2013)), it may come as no surprise that there is also considerable overlap and interconnectedness between the mid-stage input areas (PIP and CIP) of these two pathways.

Overall, we demonstrated that area PIP is a mid-level visual area critical for the neural computations involved in 3D object viewing. Our integrated approach combining fMRI, single-cell recordings and advanced analysis techniques represents a powerful research approach to clarify how cortical networks operate, how the fMRI signal relates to the properties of individual neurons and populations of neurons, and how information is represented at the different levels in the hierarchy of cortical areas.

5. **Conclusion**

The neuronal selectivity for 3D stimuli in the fMRI activation elicited by curved surfaces in PIP consists mainly of zero-and first-order neurons and a very small percentage of second-order neurons. The representation of depth structure at the population level, however, is largely higher-order. PIP cells tolerate variations in stimulus size and have parafoveal multi-focal receptive fields that are rarely centered on the fovea. We suggest that PIP may be one of the earliest higher-order disparity-processing areas in the dorsal stream.

Tested neurons	Planar	Curved
First Order	26	5*
Second Order	-	6
Zero Order	43	41
Total number of neurons tested	69	52

* These 5 neurons were also first-order when tested with the planar stimuli, and were therefore not counted as second-order neurons. Twenty-five zero-order neurons were tested with both planar and curved surfaces (43 + 41 - 25 = 59 zero-order neurons in total).

Table 1: Numbers of neurons tested with planar and curved surfaces

References

Anzai, A., Chowdhury, S.A., DeAngelis, G.C., 2011. Coding of stereoscopic depth information in visual areas V3 and V3A. J Neurosci 31, 10270-10282.

Ban, H., Welchman, A.E., 2015. fMRI Analysis-by-Synthesis Reveals a Dorsal Hierarchy That Extracts Surface Slant. J Neurosci 35, 9823-9835.

Bosco, A., Breveglieri, R., Chinellato, E., Galletti, C., Fattori, P., 2010. Reaching activity in the medial posterior parietal cortex of monkeys is modulated by visual feedback. J Neurosci 30, 14773-14785.

Cumming, B.G., DeAngelis, G.C., 2001. The physiology of stereopsis. Annu Rev Neurosci 24, 203-238.

Durand, J.-B., Nelissen, K., Joly, O., Wardak, C., Todd, J.T., Norman, J.F., Janssen, P., Vanduffel, W., Orban, G.A., 2007. Anterior Regions of Monkey Parietal Cortex Process Visual 3D Shape. Neuron 55, 493-505.

Durand, J.-B., Peeters, R., Norman, J.F., Todd, J.T., Orban, G.A., 2009. Parietal regions processing visual 3D shape extracted from disparity. NeuroImage 46, 1114-1126.

Fattori, P., Raos, V., Breveglieri, R., Bosco, A., Marzocchi, N., Galletti, C., 2010. The dorsomedial pathway is not just for reaching: grasping neurons in the medial parieto-occipital cortex of the macaque monkey. J Neurosci 30, 342-349.

Georgieva, S.S., Todd, J.T., Peeters, R., Orban, G.A., 2008. The extraction of 3D shape from texture and shading in the human brain. Cereb Cortex 18, 2416-2438.

Hadjidimitrakis, K., Bertozzi, F., Breveglieri, R., Bosco, A., Galletti, C., Fattori, P., 2014. Common neural substrate for processing depth and direction signals for reaching in the monkey medial posterior parietal cortex. Cereb Cortex 24, 1645-1657.

Hadjidimitrakis, K., Breveglieri, R., Bosco, A., Fattori, P., 2012. Three-dimensional eye position signals shape both peripersonal space and arm movement activity in the medial posterior parietal cortex. Front Integr Neurosci 6, 37.

Haufe, S., Meinecke, F., Gorgen, K., Dahne, S., Haynes, J.D., Blankertz, B., Biessmann, F., 2014. On the interpretation of weight vectors of linear models in multivariate neuroimaging. NeuroImage 87, 96-110.

Hegde, J., Van Essen, D.C., 2005. Role of primate visual area V4 in the processing of 3-D shape characteristics defined by disparity. J Neurophysiol 94, 2856-2866.

Janssen, P., Srivastava, S., Ombelet, S., Orban, G.A., 2008. Coding of shape and position in macaque lateral intraparietal area. J Neurosci 28, 6679-6690.

Janssen, P., Verhoef, B.E., Premereur, E., 2017. Functional interactions between the macaque dorsal and ventral visual pathways during three-dimensional object vision. Cortex. doi.org/10.1016/j.cortex.2017.01.021

Janssen, P., Vogels, R., Liu, Y., Orban, G.A., 2001. Macaque inferior temporal neurons are selective for three-dimensional boundaries and surfaces. J Neurosci 21, 9419-9429.

Janssen, P., Vogels, R., Orban, G.A., 1999. Macaque inferior temporal neurons are selective for disparity-defined three-dimensional shapes. Proc Natl Acad Sci U S A 96, 8217-8222.

Janssen, P., Vogels, R., Orban, G.A., 2000a. Selectivity for 3D shape that reveals distinct areas within macaque inferior temporal cortex. Science 288, 2054-2056.

Janssen, P., Vogels, R., Orban, G.A., 2000b. Three-dimensional shape coding in inferior temporal cortex. Neuron 27, 385-397.

Katsuyama, N., Yamashita, A., Sawada, K., Naganuma, T., Sakata, H., Taira, M., 2010. Functional and histological properties of caudal intraparietal area of macaque monkey. Neuroscience 167, 1-10.

Konen, C.S., Mruczek, R.E., Montoya, J.L., Kastner, S., 2013. Functional organization of human posterior parietal cortex: grasping- and reaching-related activations relative to topographically organized cortex. J Neurophysiol 109, 2897-2908.

Lehmann, S.J., Scherberger, H., 2013. Reach and gaze representations in macaque parietal and premotor grasp areas. J Neurosci 33, 7038-7049.

Lewis, J.W., Van Essen, D.C., 2000. Corticocortical connections of visual, sensorimotor, and multimodal processing areas in the parietal lobe of the macaque monkey. J Comp Neurol 428, 112-137.

Logothetis, N.K., Pauls, J., Augath, M., Trinath, T., Oeltermann, A., 2001. Neurophysiological investigation of the basis of the fMRI signal. Nature 412, 150-157.

Meyers, E.M., Freedman, D.J., Kreiman, G., Miller, E.K., Poggio, T., 2008. Dynamic population coding of category information in inferior temporal and prefrontal cortex. J Neurophysiol 100, 1407-1419.

Murata, A., Gallese, V., Luppino, G., Kaseda, M., Sakata, H., 2000. Selectivity for the shape, size, and orientation of objects for grasping in neurons of monkey parietal area AIP. J Neurophysiol 83, 2580-2601.

Nakamura, H., Kuroda, T., Wakita, M., Kusunoki, M., Kato, A., Mikami, A., Sakata, H., Itoh, K., 2001. From three-dimensional space vision to prehensile hand movements: the lateral intraparietal area links the area V3A and the anterior intraparietal area in macaques. J Neurosci 21, 8174-8187.

Orban, G.A., 2011. The extraction of 3D shape in the visual system of human and nonhuman primates. Annu Rev Neurosci 34, 361-388.

Orban, G.A., 2016. Functional definitions of parietal areas in human and non-human primates. Proc Biol Sci 283.

Parker, A.J., 2007. Binocular depth perception and the cerebral cortex. Nature Reviews. Neuroscience 8, 379-391.

Popivanov, I.D., Jastorff, J., Vanduffel, W., Vogels, R., 2012. Stimulus representations in body-selective regions of the macaque cortex assessed with event-related fMRI. NeuroImage 63, 723-741.

Premereur, E., Van Dromme, I.C., Romero, M.C., Vanduffel, W., Janssen, P., 2015. Effective connectivity of depth-structure-selective patches in the lateral bank of the macaque intraparietal sulcus. PLoS Biol 13, e1002072.

Romero, M.C., Janssen, P., 2016. Receptive field properties of neurons in the macaque anterior intraparietal area. J Neurophysiol 115, 1542-1555.

Rosenberg, A., Angelaki, D.E., 2014a. Gravity influences the visual representation of object tilt in parietal cortex. J Neurosci 34, 14170-14180.

Rosenberg, A., Angelaki, D.E., 2014b. Reliability-dependent contributions of visual orientation cues in parietal cortex. Proc Natl Acad Sci U S A 111, 18043-18048.

Rosenberg, A., Cowan, N.J., Angelaki, D.E., 2013. The visual representation of 3D object orientation in parietal cortex. J Neurosci 33, 19352-19361.

Sakata, H., Tsutsui, K., Taira, M., 2005. Toward an understanding of the neural processing for 3D shape perception. Neuropsychologia 43, 151-161.

Shikata, E., McNamara, A., Sprenger, A., Hamzei, F., Glauche, V., Buchel, C., Binkofski, F., 2008. Localization of human intraparietal areas AIP, CIP, and LIP using surface orientation and saccadic eye movement tasks. Hum Brain Mapp 29, 411-421.

Srivastava, S., Orban, G.A., Mazière, P.A.D., Janssen, P., 2009. A Distinct Representation of Three-Dimensional Shape in Macaque Anterior Intraparietal Area: Fast, Metric, and Coarse. The Journal of Neuroscience 29, 10613-10626.

Taira, M., Tsutsui, K.I., Jiang, M., Yara, K., Sakata, H., 2000. Parietal neurons represent surface orientation from the gradient of binocular disparity. J Neurophysiol 83, 3140-3146.

Theys, T., Pani, P., van Loon, J., Goffin, J., Janssen, P., 2012a. Selectivity for three-dimensional shape and grasping-related activity in the macaque ventral premotor cortex. J Neurosci 32, 12038-12050.

Theys, T., Pani, P., van Loon, J., Goffin, J., Janssen, P., 2013. Three-dimensional shape coding in grasping circuits: a comparison between the anterior intraparietal area and ventral premotor area F5a. J Cogn Neurosci 25, 352-364.

Theys, T., Srivastava, S., van Loon, J., Goffin, J., Janssen, P., 2012b. Selectivity for three-dimensional contours and surfaces in the anterior intraparietal area. J Neurophysiol 107, 995-1008.

Thomas, O.M., Cumming, B.G., Parker, A.J., 2002. A specialization for relative disparity in V2. Nat Neurosci 5, 472-478.

Tsao, D.Y., Vanduffel, W., Sasaki, Y., Fize, D., Knutsen, T.A., Mandeville, J.B., Wald, L.L., Dale, A.M., Rosen, B.R., Van Essen, D.C., Livingstone, M.S., Orban, G.A., Tootell, R.B., 2003. Stereopsis activates V3A and caudal intraparietal areas in macaques and humans. Neuron 39, 555-568.

Tsutsui, K., Jiang, M., Yara, K., Sakata, H., Taira, M., 2001. Integration of perspective and disparity cues in surface-orientation-selective neurons of area CIP. J Neurophysiol 86, 2856-2867.

Tsutsui, K., Sakata, H., Naganuma, T., Taira, M., 2002. Neural correlates for perception of 3D surface orientation from texture gradient. Science 298, 409-412.

Van Dromme, I.C., Premereur, E., Verhoef, B.E., Vanduffel, W., Janssen, P., 2016. Posterior Parietal Cortex Drives Inferotemporal Activations During Three-Dimensional Object Vision. PLoS Biol 14, e1002445.

Van Dromme, I.C., Vanduffel, W., Janssen, P., 2015. The relation between functional magnetic resonance imaging activations and single-cell selectivity in the macaque intraparietal sulcus. NeuroImage 113, 86-100.

Verhoef, B.E., Vogels, R., Janssen, P., 2012. Inferotemporal cortex subserves three-dimensional structure categorization. Neuron 73, 171-182.

Yamane, Y., Carlson, E.T., Bowman, K.C., Wang, Z., Connor, C.E., 2008. A neural code for three-dimensional object shape in macaque inferotemporal cortex. Nat Neurosci 11, 1352-1360.

Zhao, F., Wang, P., Hendrich, K., Ugurbil, K., Kim, S.G., 2006. Cortical layer-dependent BOLD and CBV responses measured by spin-echo and gradient-echo fMRI: insights into hemodynamic regulation. NeuroImage 30, 1149-1160.

Figure legends

Figure 1. Stimuli. **A**. Random-dot stereogram of a planar surface with the top part tilted towards the observer (red in front of left eye in anaglyphs). Planar surfaces were either rotated along the horizontal axis (disparity variation along the vertical axis of the surface) or rotated along the vertical axis (disparity variation along the horizontal axis). **B**. Two-dimensional contours (top) and three-dimensional profiles (bottom) used to create curved (second-order) surfaces defined

solely by gradients of binocular disparity along the vertical axis of the shape. The icon on the far right is a rendering of the perceived stimulus. No perspective or shading information was present in the stimuli used in this experiment.

Figure 2. fMRI results and recording positions. **A**. Significant fMRI activations related to depth structure (interaction between curvature and disparity) in the caudal Intraparietal Sulcus of monkey A., mapped on two coronal sections of the monkey's own anatomical MRI. The black line in the top panel is an electrode in one of the recording positions. The labels for the other fMRI activations are indicated on the recorded hemisphere only. PIP: Posterior Intraparietal area. V4: visual area V4. LIPd: dorsal Lateral Intraparietal area. CIP: Caudal Intraparietal area. A-P denotes the anterior-posterior stereotactic coordinate of the coronal section. **B**. Top panel: recording sites mapped onto a horizontal section with fMRI activation. The color of each grid position indicates the percentage of disparity-selective cells. The red cross indicates the center of the grid. Lower panel: dorsolateral view of the macaque brain showing the anterior-posterior level of the recordings (blue lines). **C** and **D**. Same results for monkey R.

Figure 3. Disparity selectivity in area PIP. **A**. Peristimulus-time histogram (PSTH) of an example PIP neuron tested with planar surfaces in the stereo condition ('Stereo') and in the monocular conditions ('Left Eye' and 'Right Eye'). The horizontal bar indicates the first 400 ms after stimulus onset (total duration of stimulus presentation was 600 ms). **B**. PSTH of the same neuron tested with curved surfaces. Same conventions as in A. Vertical and horizontal calibration bars represent spikes/sec and time in milliseconds respectively in panel A and B. **C**. Average population response (+/- SE) to preferred (blue) and nonpreferred (red) planar surfaces of all PIP neurons selective for planar surfaces (N= 74). The dashed lines indicate the monocular responses (black: preferred right eye, green: nonpreferred right eye, cyan: preferred left eye, purple: nonpreferred left eye). **D**. Average population response to preferred (blue) and nonpreferred (red) curved surfaces of all PIP neurons selective for curved surfaces (N = 54).

Same conventions as in C. **E**. Distribution of the SSI for planar (blue bars) and curved (red bars) stimuli. The SIs of the example neuron for planar and curved stimuli are indicated on the histogram with blue and red arrows, respectively.

Figure 4. Position-in-depth test, example neuron. **A.** PSTHs of the example neuron in the position-in-depth test with planar surfaces. The preferred (top row) and the nonpreferred (bottom row) planar surfaces were presented at 5 different positions in depth (-0.5° indicates near disparities, whereas +0.5° indicates far disparities). Same conventions as in Figure 3. **B**. PSTH of the same example neuron in the position-in-depth test with curved surfaces. Vertical and horizontal calibration bars represent spikes/sec and time in milliseconds respectively in panels A and B. **C**. Average horizontal eye position traces (red: right eye, blue: left eye) at three positions-in-depth (near, fixation plane and far) recorded together with the example neuron. The vertical scale bar on the left indicates 1°. Horizontal calibration bars indicate time in milliseconds.

Figure 5. Position-in-depth test, population analysis. **A**. Average normalized net response to preferred (blue) and nonpreferred (red) planar surface in the position-in-depth test for all higher-order PIP neurons (N = 26). **B**. Average normalized net response to preferred (blue) and nonpreferred (red) curved surface in the position-in-depth test for all higher-order PIP neurons tested with curved surfaces (N = 11). **C**. Scatterplot illustrating the Selectivity index at the middle position (on the x-axis) as a function of the Selectivity Index at the worst position (on the y-axis), for first-order (blue), second-order (black) and zero-order (red) neurons. Green symbols indicate the first-order and zero-order neurons tested with curved surfaces. **D**. Average net response to the preferred and to the nonpreferred stimulus for curved (red), planar (blue) and flat (black line) surfaces of all disparity-selective PIP neurons (N= 61) at three positions in depth, which was the same range as in the fMRI experiment. (* $P<0.05$, ** $P<0.01$ and ***

P<0.001). In correspondence with the fMRI experiment, we averaged the responses to preferred and nonpreferred surfaces.

Figure 6. Size test. **A.** Average net responses of an example neuron to the preferred (blue) and nonpreferred (black) planar surface at eight different sizes. **B**. Average normalized net responses of all PIP neurons (N=40) tested with different sizes (preferred: blue, nonpreferred surface: red). (* *P*<0.05, ** *P*<0.01 and *** *P*<0.001)

Figure 7. Receptive fields of PIP neurons. **A.** Example neuron's receptive field with a single parafoveal maximum. The color indicates the average net response of the neuron at each position. The red line indicates the response level at -1 SD from the RF maximum. **B.** Example neuron's receptive field with two parafoveal maxima in either hemifield. Same conventions as in A. **C.** Example neuron's receptive field with two parafoveal maxima in either hemifield located farther away from the fovea. **D.** Average receptive field of all disparity-selective PIP neurons tested (N=40). The color bar indicates normalized net response.

Figure 8. Decoding analysis. **A**. Classification accuracy for the sign of the disparity gradient of planar (green bar) and curved (blue bar) surfaces. **B.** Classification accuracy for the position in depth (near, fixation plane or far) for planar (green bar) and curved (blue bar) surfaces. **C.** Generalization analysis results matrix for planar surfaces. The p-values (indicated by colors) illustrate how reliably the classifier could classify the sign of the disparity gradient at one position in depth when trained at another positon in depth. A red line in the color bar indicates chance level. **D.** Results of the generalization analysis for curved surfaces. Same conventions as in C.

8. Table

Tested neurons	Planar	Curved
First Order	26	5*
Second Order	-	6
Zero Order	43	41
Total number of neurons tested	69	52

* These 5 neurons were also first-order when tested with the planar stimuli, and were therefore not counted as second-order neurons. Twenty-five zero-order neurons were tested with both planar and curved surfaces (43 + 41 - 25 = 59 zero-order neurons in total).

Table 1: Numbers of neurons tested with planar and curved surfaces

9. Figure

Click here to download 9. Figure: PIP FIGURES final.pdf

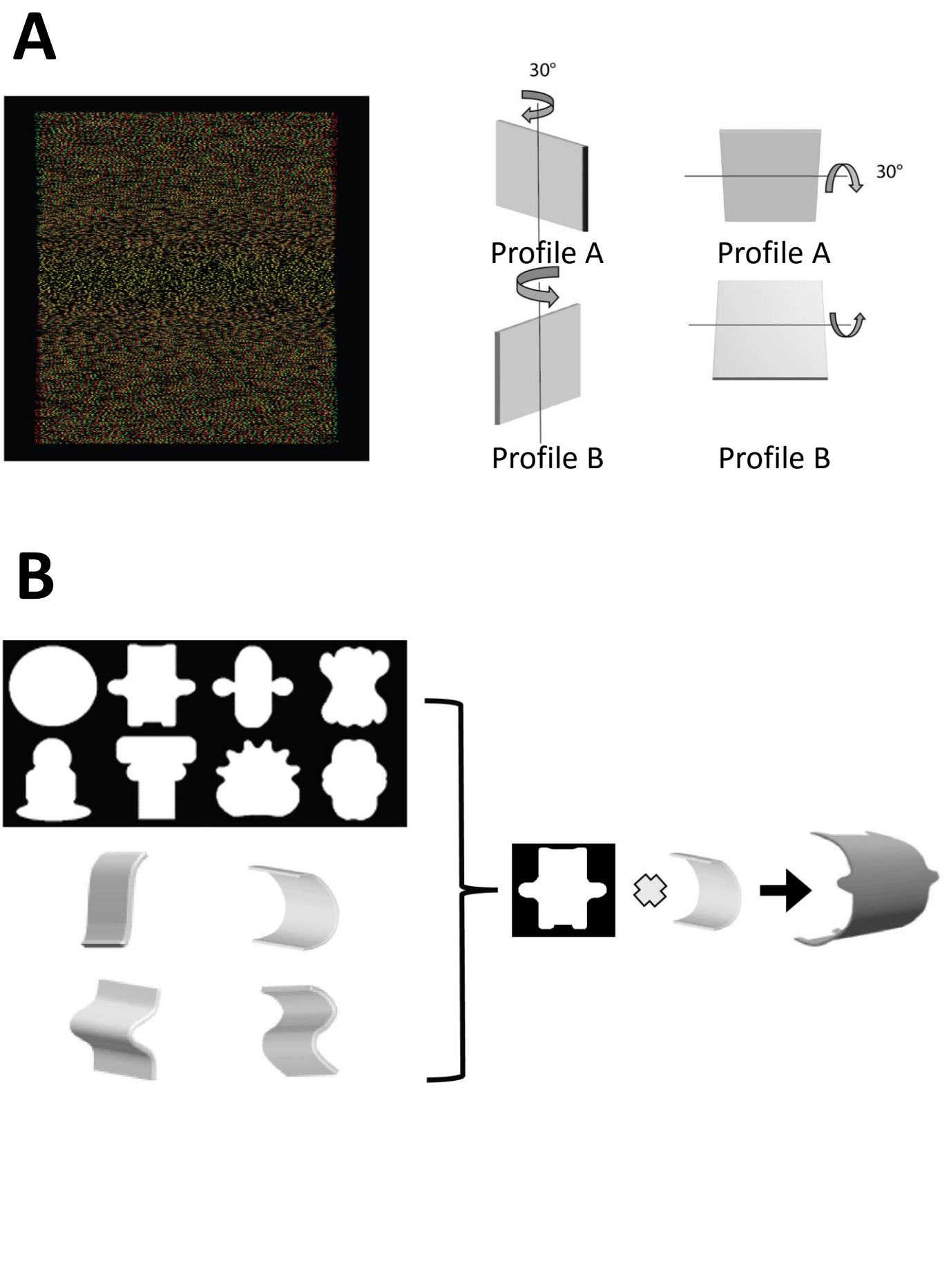

Figure 1. Stimuli. **A**. Random-dot stereogram of a planar surface with the top part tilted towards the observer (red in front of left eye in anaglyphs). Planar surfaces were either rotated along the horizontal axis (disparity variation along the vertical axis of the surface) or rotated along the vertical axis (disparity variation along the horizontal axis). **B**. Two-dimensional contours (top) and three-dimensional profiles (bottom) used to create curved (second-order) surfaces defined solely by gradients of binocular disparity along the vertical axis of the shape. The icon on the far right is a rendering of the perceived stimulus. No perspective or shading information was present in the stimuli used in this experiment.

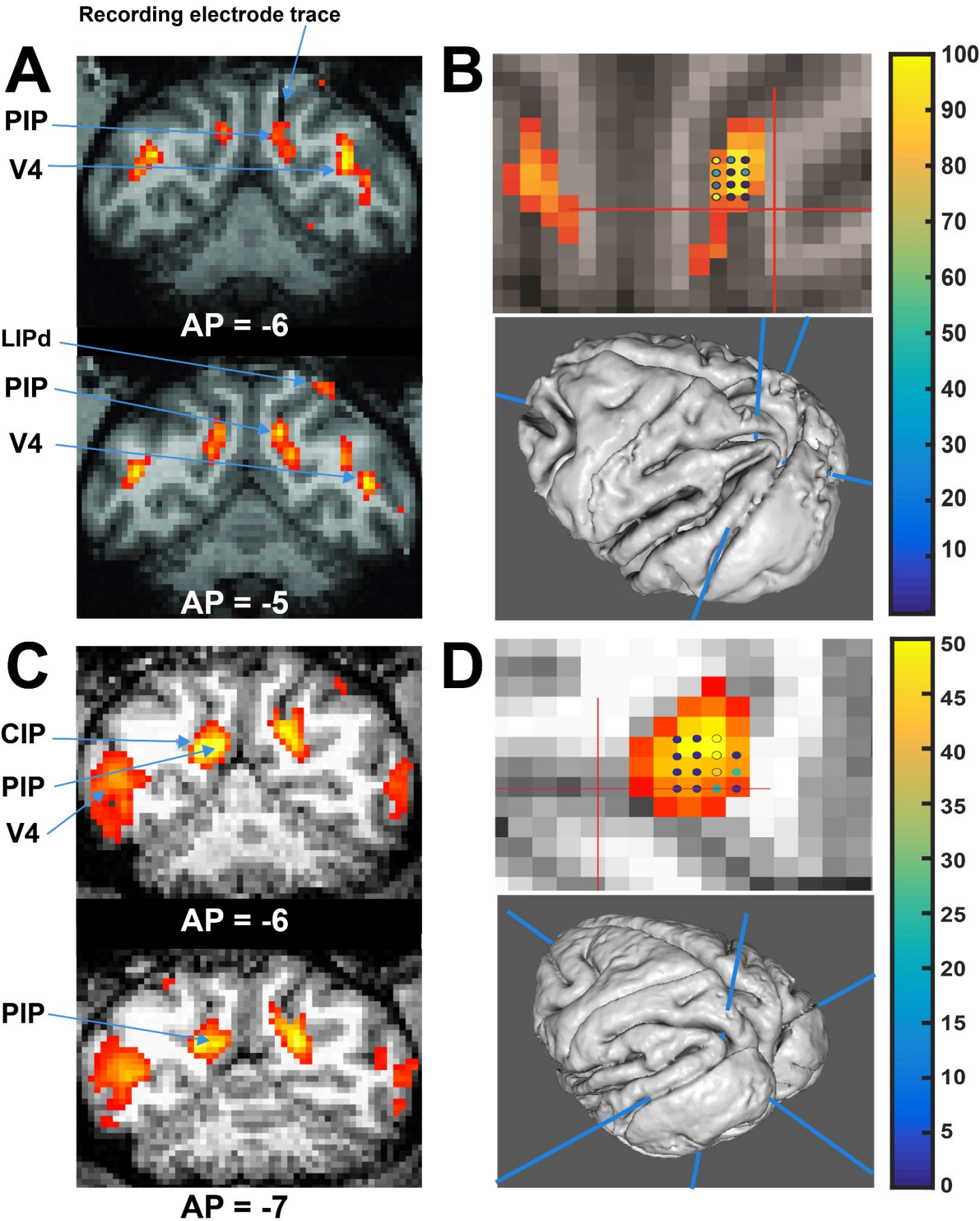
Recording electrode trace
A
PIP
V4
AP = -6
LIPd
PIP
V4
AP = -5
B
100
90
80
70
60
50
40
30
20
10
C
CIP
PIP
V4
AP = -6
PIP
AP = -7
D
50
45
40
35
30
25
20
15
10
5
0

Figure 2. fMRI results and recording positions. **A**. Significant fMRI activations related to depth structure (interaction between curvature and disparity) in the caudal Intraparietal Sulcus of monkey A., mapped on two coronal sections of the monkey's own anatomical MRI. The black line in the top panel is an electrode in one of the recording positions. The labels for the other fMRI activations are indicated on the recorded hemisphere only. PIP: Posterior Intraparietal area. V4: visual area V4. LIPd: dorsal Lateral Intraparietal area. CIP: Caudal Intraparietal area. A-P denotes the anterior-posterior stereotactic coordinate of the coronal section. **B.** Top panel: recording sites mapped onto a horizontal section with fMRI activation. The color of each grid position indicates the percentage of disparity-selective cells. The red cross indicates the center of the grid. Lower panel: dorsolateral view of the macaque brain showing the anterior-posterior level of the recordings (blue lines). **C and D**. Same results for monkey R.

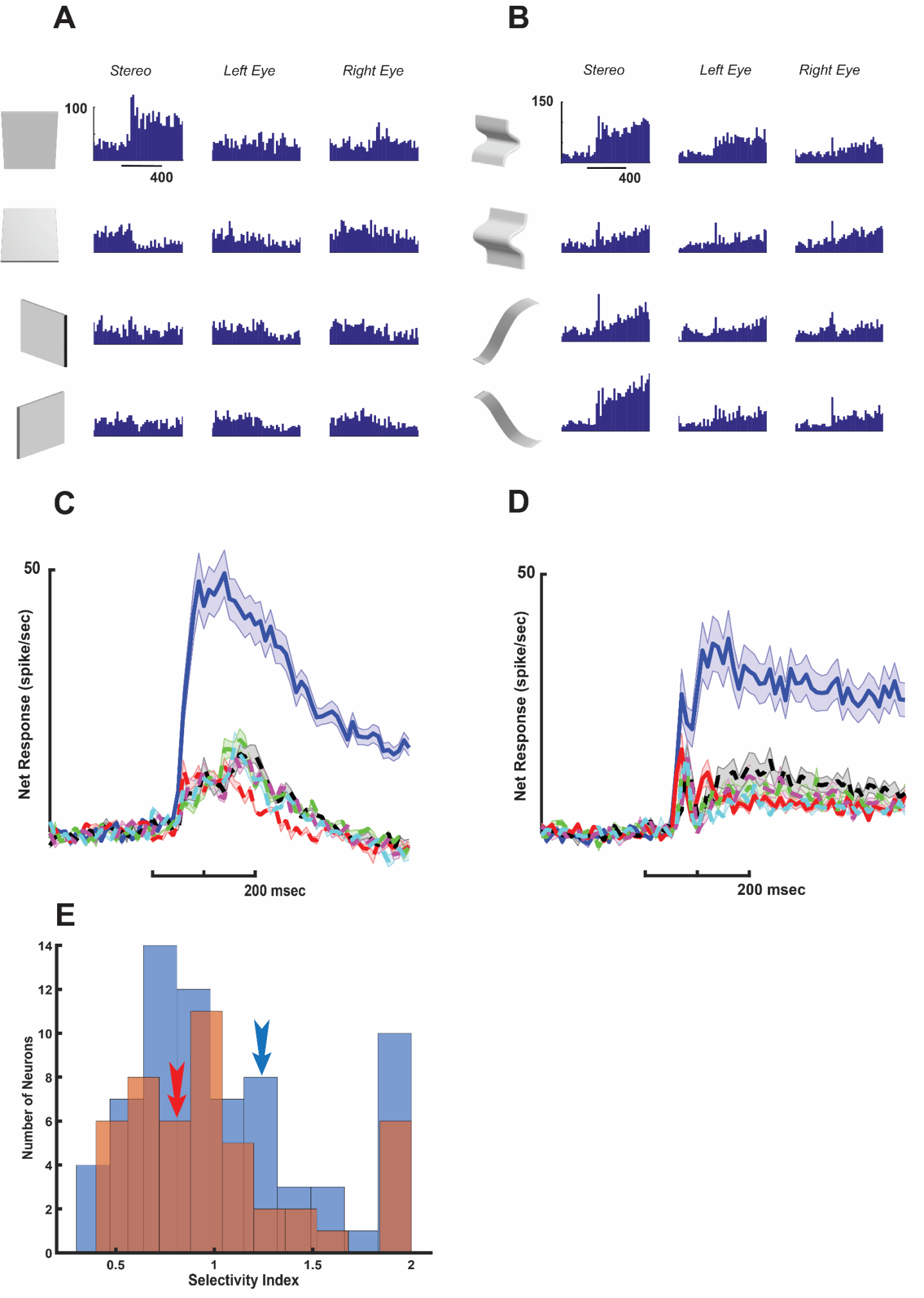
A
Stereo
Left Eye
Right Eye
100
400
B
Stereo
Left Eye
Right Eye
150
400
C
50
Net Response (spike/sec)
200 msec
D
50
Net Response (spike/sec)
200 msec
E
14
12
10
8
6
4
2
0
Number of Neurons
0.5
1
1.5
2
Selectivity Index

Figure 3. Disparity selectivity in area PIP. **A.** Peristimulus-time histogram (PSTH) of an example PIP neuron tested with planar surfaces in the stereo condition ('Stereo') and in the monocular conditions ('Left Eye' and 'Right Eye'). The horizontal bar indicates the first 400 ms after stimulus onset (total duration of stimulus presentation was 600 ms). **B.** PSTH of the same neuron tested with curved surfaces. Same conventions as in A. Vertical and horizontal calibration bars represent spikes/sec and time in milliseconds respectively in panel A and B. **C.** Average population response (+/- SE) to preferred (blue) and nonpreferred (red) planar surfaces of all PIP neurons selective for planar surfaces (N= 74). The dashed lines indicate the monocular responses (black: preferred right eye, green: nonpreferred right eye, cyan: preferred left eye, purple: nonpreferred left eye). **D.** Average population response to preferred (blue) and nonpreferred (red) curved surfaces of all PIP neurons selective for curved surfaces (N = 54). Same conventions as in C. **E** Distribution of the SSI for planar (blue bars) and curved (red bars) stimuli. The SIs of the example neuron for planar and curved stimuli are indicated on the histogram with blue and red arrows, respectively.

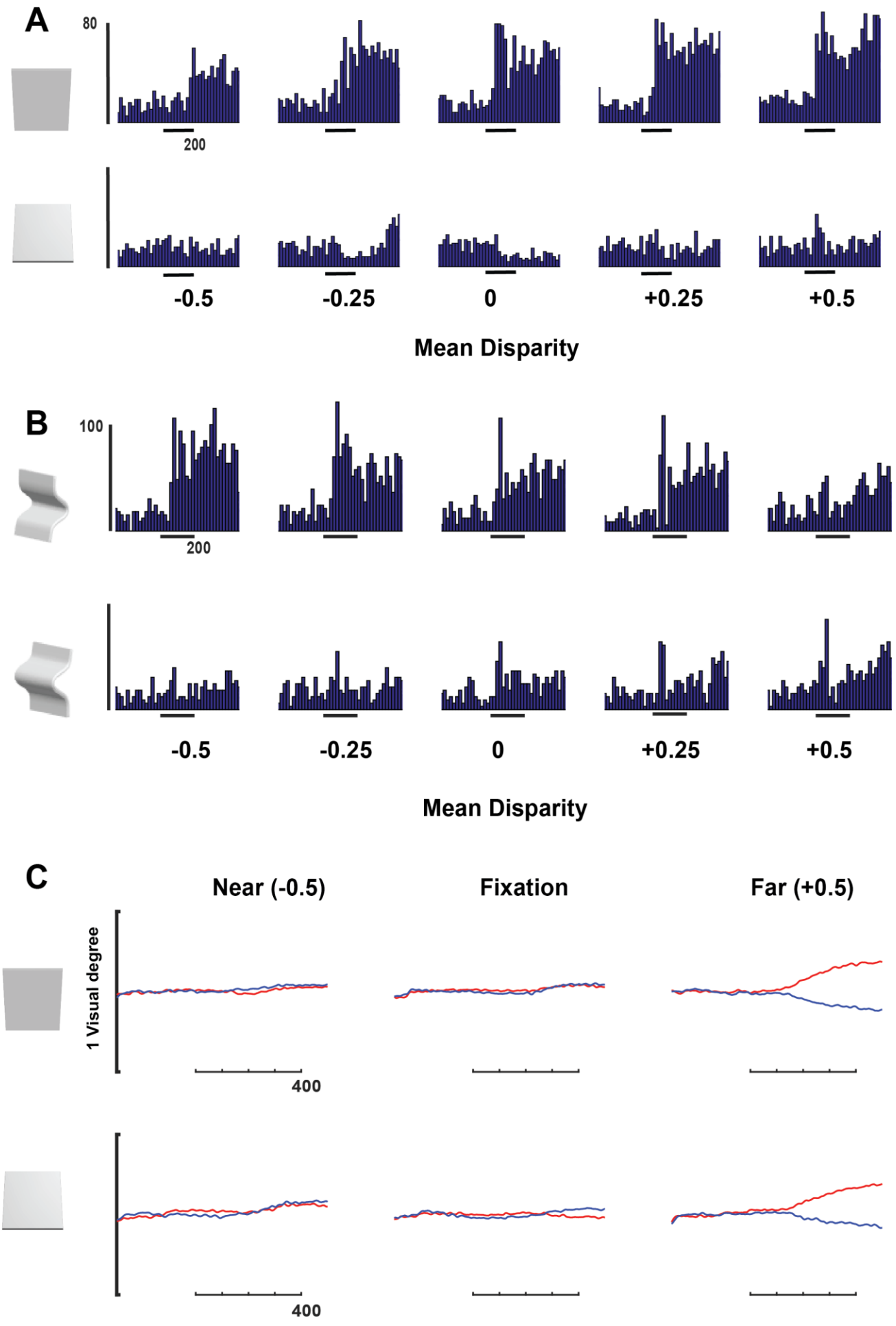
A
80
200
-0.5
-0.25
0
+0.25
+0.5
Mean Disparity
B
100
200
-0.5
-0.25
0
+0.25
+0.5
Mean Disparity
C
Near (-0.5)
Fixation
Far (+0.5)
1 Visual degree
400
400

Figure 4. Position-in-depth test, example neurons. **A.** PSTHs of the example neuron in the position-in-depth test with planar surfaces. The preferred (top row) and the nonpreferred (bottom row) planar surfaces were presented at 5 different positions in depth (-0.5° indicates near disparities, whereas +0.5° indicates far disparities). Same conventions as in Figure 3. **B.** PSTH of the same example neuron in the position-in-depth test with curved surfaces. Vertical and horizontal calibration bars represent spikes/sec and time in milliseconds respectively in panel A and B. **C.** Average horizontal eye position traces (red: right eye, blue: left eye) at three positions-in-depth (near, fixation plane and far) recorded together with the example neuron. The vertical scale bar on the left indicates 1°. Horizontal calibration bars indicate time in milliseconds.

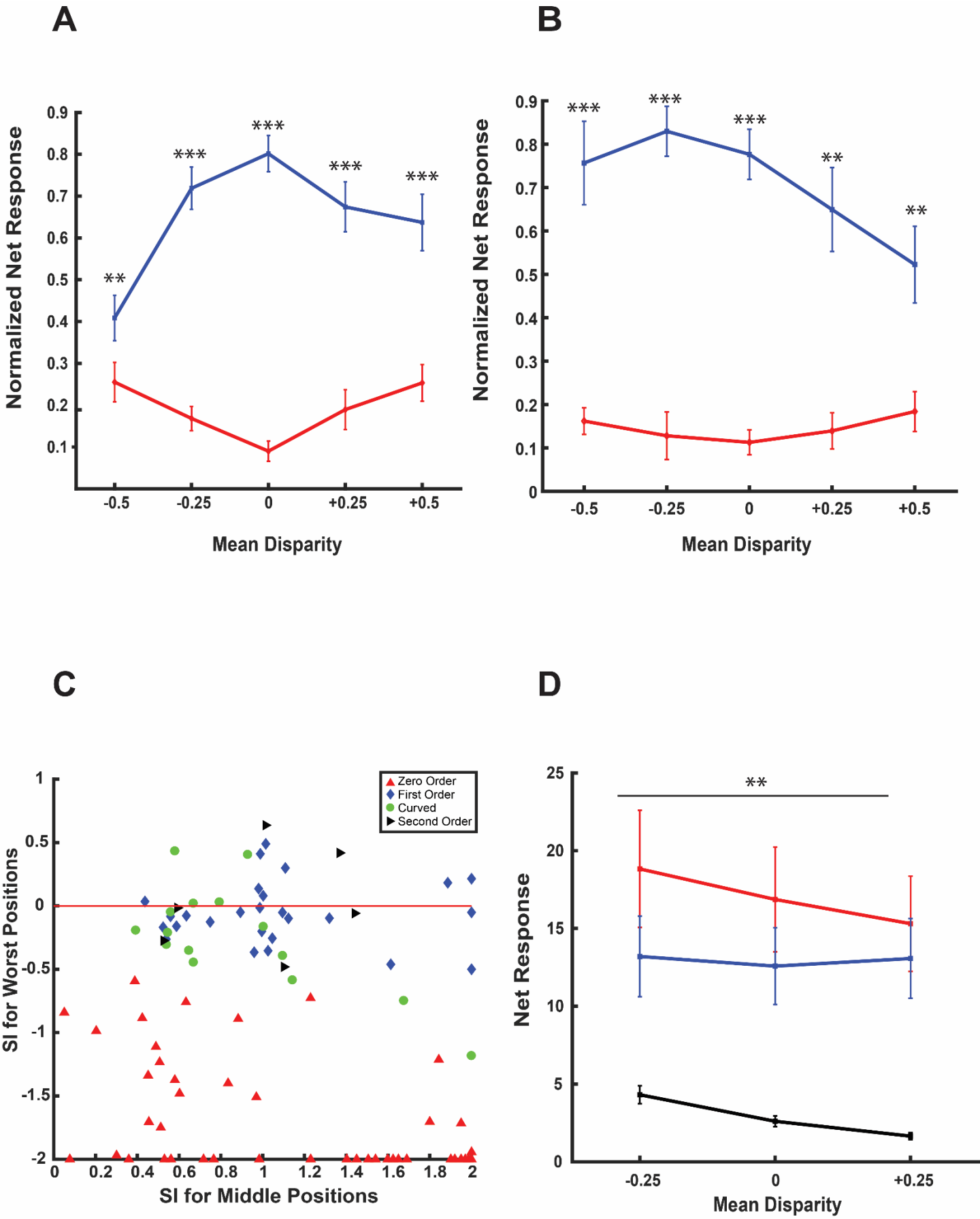
A
B
C
D
Normalized Net Response
Mean Disparity
-0.5
-0.25
0
+0.25
+0.5
**
***
Zero Order
First Order
Curved
Second Order
SI for Worst Positions
SI for Middle Positions
Net Response

Figure 5. Position-in-depth test, population analysis. **A.** Average normalized net response to preferred (blue) and nonpreferred (red) planar surface in the position-in-depth test for all higher-order PIP neurons (N = 26). **B.** Average normalized net response to preferred (blue) and nonpreferred (red) curved surface in the position-in-depth test for all higher-order PIP neurons tested with curved surfaces (N = 11). **C.** Scatterplot illustrating the Selectivity index at the middle position (on the x-axis) as a function of the Selectivity Index at the worst position (on the y-axis), for first-order (blue), second-order (black) and zero-order (red) neurons. Green symbols indicate the first-order and zero-order neurons tested with curved surfaces. **D.** Average net response to the preferred and to the nonpreferred stimulus for curved (red), planar (blue) and flat (black line) surfaces of all disparity-selective PIP neurons (N= 61) at three positions in depth, which was the same range as in the fMRI experiment. (* $P<0.05$, ** $P<0.01$ and *** $P<0.001$). In correspondence with the fMRI experiment, we averaged the responses to preferred and nonpreferred surfaces.

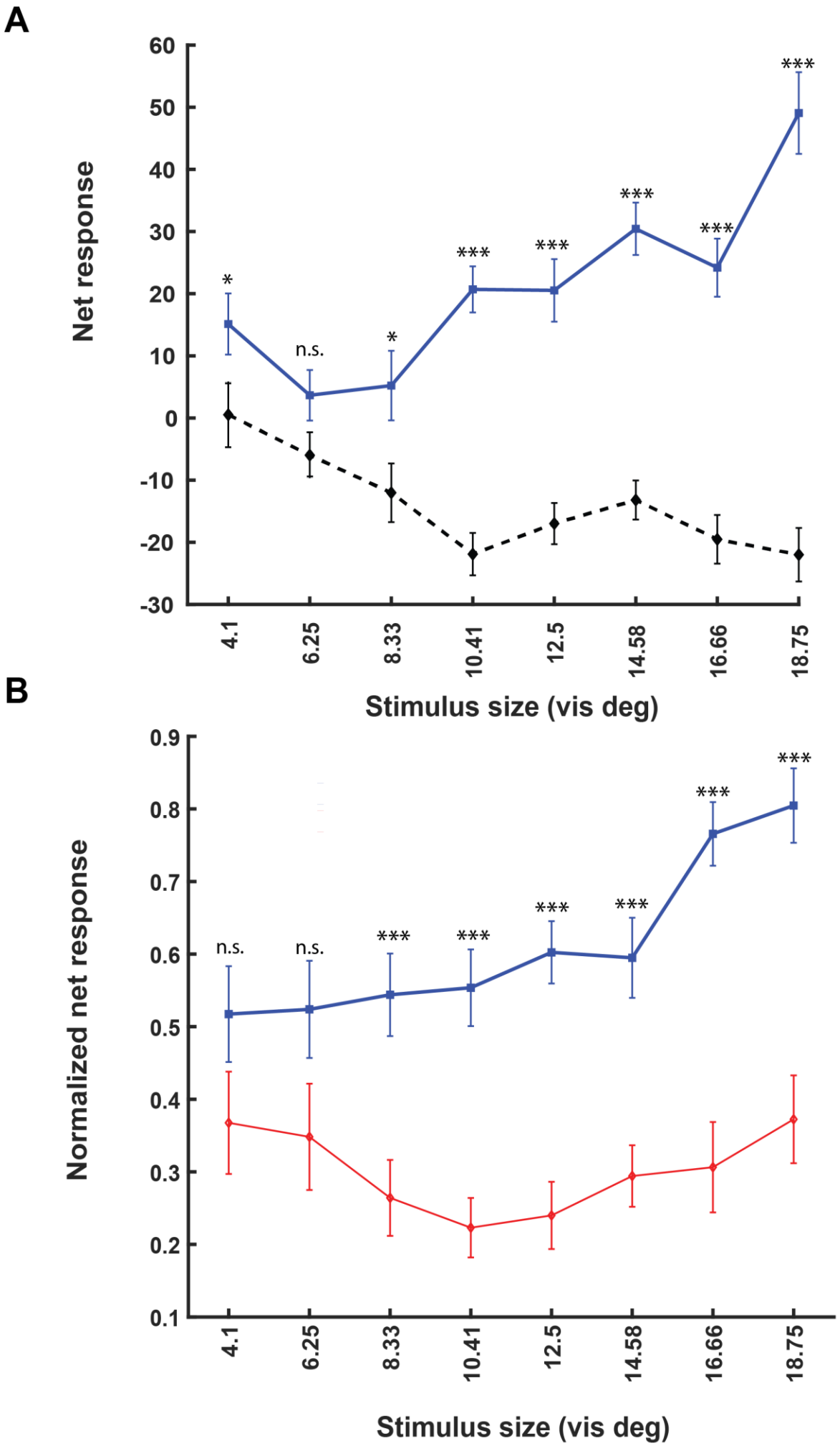
A
Net response
60
50
40
30
20
10
0
-10
-20
-30
*
n.s.
*
***
***
***
***
***
4.1
6.25
8.33
10.41
12.5
14.58
16.66
18.75
Stimulus size (vis deg)
B
Normalized net response
0.9
0.8
0.7
0.6
0.5
0.4
0.3
0.2
0.1
n.s.
n.s.
***
***
***
***
***
4.1
6.25
8.33
10.41
12.5
14.58
16.66
18.75
Stimulus size (vis deg)

Figure 6. Size test. **A.** Average net responses of an example neuron to the preferred (blue) and nonpreferred (black) planar surface at eight different sizes. **B.** Average normalized net responses of all PIP neurons (N=40) tested with different sizes (preferred: blue, nonpreferred surface: red). (* $P<0.05$, ** $P<0.01$ and *** $P<0.001$)

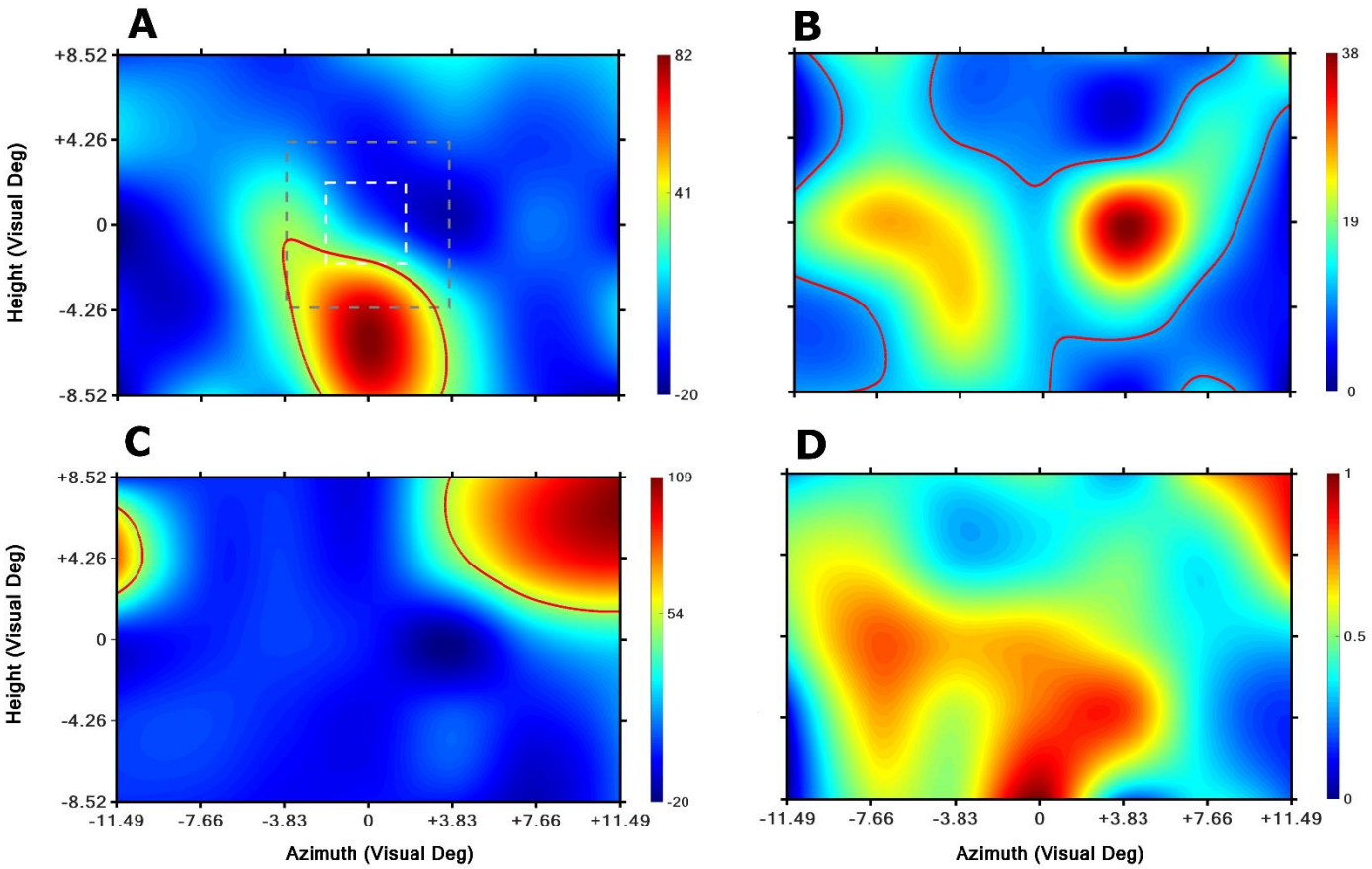
A
B
C
D
+8.52
+4.26
0
-4.26
-8.52
Height (Visual Deg)
82
41
-20
38
19
0
109
54
-20
1
0.5
0
-11.49
-7.66
-3.83
0
+3.83
+7.66
+11.49
Azimuth (Visual Deg)

Figure 7. Receptive fields of PIP neurons. A. Example neuron's receptive field with a single parafoveal maximum. The color indicates the average net response of the neuron at each position. The red line indicates the response level at -1 SD from the RF maximum. **B.** Example neuron's receptive field with two parafoveal maxima in either hemifield. Same conventions as in A. **C.** Example neuron's receptive field with two parafoveal maxima in either hemifield located farther away from the fovea. **D.** Average receptive field of all disparity-selective PIP neurons tested (N=40). The color bar indicates normalized net response.

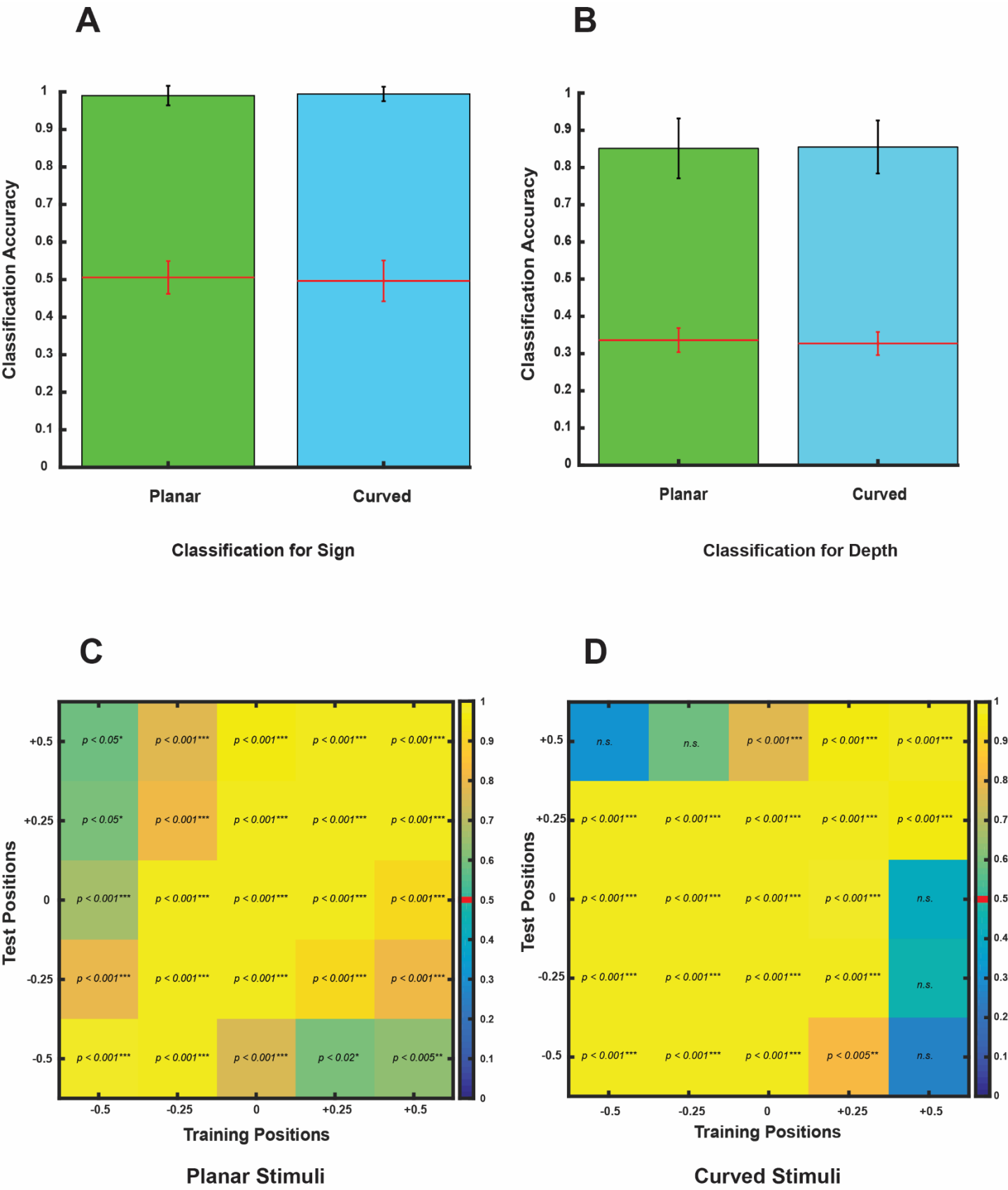
A
B
Classification Accuracy
1
0.9
0.8
0.7
0.6
0.5
0.4
0.3
0.2
0.1
0
Planar
Curved
Classification for Sign
Classification for Depth
C
D
Test Positions
+0.5
+0.25
0
-0.25
-0.5
p < 0.05*
p < 0.001***
p < 0.02*
p < 0.005**
n.s.
Training Positions
Planar Stimuli
Curved Stimuli

Figure 8. Decoding analysis. **A.** Classification accuracy for the sign of the disparity gradient of planar (green bar) and curved (blue bar) surfaces. **B.** Classification accuracy for the position in depth (near, fixation plane or far) for planar (green bar) and curved (blue bar) surfaces. **C.** Generalization analysis results matrix for planar surfaces. The p-values (indicated by colors) illustrate how reliably the classifier could classify the sign of the disparity gradient at one position in depth when trained at another positon in depth. A red line in the color bar indicates chance level. **D.** Results of the generalization analysis for curved surfaces. Same conventions as in C.

10. Supplementary Material

Click here to download 10. Supplementary Material: supplemental material.pdf